

Runge-Kutta discontinuous Galerkin method for reactive multiphase flows

Erwin Franquet, Vincent Perrier

▶ **To cite this version:**

Erwin Franquet, Vincent Perrier. Runge-Kutta discontinuous Galerkin method for reactive multiphase flows. Computers and Fluids, 2013, 83, pp.157-163. 10.1016/j.compfluid.2012.07.011 . hal-00788235

HAL Id: hal-00788235

https://inria.hal.science/hal-00788235

Submitted on 14 Feb 2013

HAL is a multi-disciplinary open access archive for the deposit and dissemination of scientific research documents, whether they are published or not. The documents may come from teaching and research institutions in France or abroad, or from public or private research centers.

L'archive ouverte pluridisciplinaire **HAL**, est destinée au dépôt et à la diffusion de documents scientifiques de niveau recherche, publiés ou non, émanant des établissements d'enseignement et de recherche français ou étrangers, des laboratoires publics ou privés.

Runge-Kutta discontinuous Galerkin method for reactive multiphase flows

Erwin Franquet[a,b,*], Vincent Perrier[b,c]

[a] *LaTEP-ENSGTI, Université de Pau et des Pays de l'Adour, Bâtiment d'Alembert, rue Jules Ferry, 64 075 Pau Cedex*
[b] *INRIA Bordeaux Sud Ouest,* Cagire *Team, 351 Cours de la Libération, 33 405 Talence Cedex*
[c] *LMA-IPRA, UMR CNRS 5142, Université de Pau et des Pays de l'Adour, Avenue de l'Université, 64 013 Pau Cedex*

Abstract

A Runge-Kutta discontinuous Galerkin method is developed for the modeling of reactive compressible multiphase flows. From the work developed in [1], where a discontinuous Galerkin formulation was obtained for inert flows based on the ideas of [2] and [3], we introduce a reactive Riemann problem [4] so as to take into account the reactions we are interested in (*i.e.* reactions with infinitely fast time rates). Several reactive examples are presented. The corresponding results show the high capabilities of the method, which can simulate the strong density and pressure ratios, and also has no problem whenever a phase appears or disappears.

Keywords: reactive compressible multiphase flow, Runge-Kutta discontinuous Galerkin method, high order method, phase transition, detonation.

1. Introduction

In this article, we propose an extension of the discontinuous Galerkin (dG) method developed in [1] to reactive compressible multi-material flows. Among the issues raised by inert compressible multiphase flows (non-conservative terms, closure, hyperbolicity...) [5, 6, 7, 8], we want to address the difficulty

*Corresponding author
Email address: erwin.franquet@univ-pau.fr (Erwin Franquet)

of dealing with reactions into such flows. Usually, we may find two approaches: either the reaction zone is explicitly solved or implicitly taken into account with another method. A direct modeling should consist in adding a mass fraction equation involving a source term, which accounts for the reaction. Yet this source term is often very stiff, inducing a strong limitation on the time step while performing its numerical time integration by an explicit scheme. When the reactions are very fast, they may be represented as discontinuous fronts and it is then possible to consider them as waves in the Riemann problem and thus to insert them in a Godunov type method [4].

Our starting point is a Baer and Nunziato type model [5], which is able to model both interface problems and multiphase mixtures. With these models, the numerical discretization usually supposes that the interface is a diffuse zone, where the volume fraction is strictly between 0 and 1 (the first case corresponding to the absence of the associated fluid and the second to the case where it is pure). Our aim in this study is thus to show the capabilities of a Runge-Kutta discontinuous Galerkin method [9] to deal with reactive compressible multiphase flows, where reactions are supposed to be very fast and are consequently integrated as reactive fronts in the Riemann problem [4]. We use the discrete equations method [2] to deal with the convective fluxes and implement a reactive Riemann problem. The paper is organized as follows. In Section 2, we first present the corresponding modeling for the situations we have in mind (i.e. detonation waves and phase transitions modeled by an isothermal van-der-Waals equation of state). In Section 3, we show how to obtain a discontinuous Galerkin discretization for the corresponding model. Finally, numerical results, both one-dimensional and two-dimensional, are presented in Section 4.

2. Physical model

This study aims at modeling permeable fronts, *e.g.* detonation waves and phase transitions.

2.1. Governing Equations

Compressible multi-material flows are represented by the so-called Baer and Nunziato type models [5]:

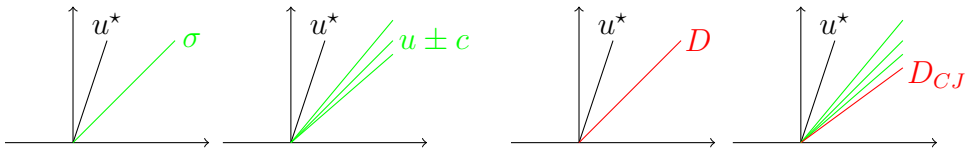
$$\begin{aligned}
&\frac{\partial \alpha_k}{\partial t} + \mathbf{u}_I \cdot \nabla \alpha_k = 0 \\
&\frac{\partial \left(\alpha_k \rho_k\right)}{\partial t} + \text{div } \left(\alpha_k \rho_k \mathbf{u}_k\right) = 0 \\
&\frac{\partial \left(\alpha_k \rho_k \mathbf{u}_k\right)}{\partial t} + \text{div } \left(\alpha_k \rho_k \mathbf{u}_k \otimes \mathbf{u}_k\right) + \nabla(\alpha_k P_k) = P_I \nabla \alpha_k \\
&\frac{\partial \left(\alpha_k \rho_k E_k\right)}{\partial t} + \text{div } \left(\alpha_k \left(\rho_k E_k + P_k\right) \mathbf{u}_k\right) = P_I \mathbf{u}_I \cdot \nabla \alpha_k
\end{aligned} \tag{1}$$

Here, $\alpha_k, \rho_k, \mathbf{u}_k, P_k, E_k$ denote the volume fraction, density, velocity, static pressure, and total energy of the phase k. As usual, the thermodynamic parameters are linked together thanks to the equation of state $\varepsilon_k = \varepsilon_k(P_k, \rho_k)$ where ε_k is the internal energy, deduced from the total energy $\varepsilon_k = E_k - \frac{\mathbf{u}_k \cdot \mathbf{u}_k}{2}$. Eventually, $\mathbf{u}_I$ and P_I are the interfacial velocity and pressure. Their definition can raise problems, but we will not need to explicitly define them in our numerical method.

Concerning the source terms that appear when reactive effects are considered, we will suppose that the reactive fronts behave as discontinuous fronts. Therefore, the reactive zone will not be directly integrated as for example in [10]. Instead, we will solve a reactive Riemann problem which incorporates these reactive fronts, as proposed by [4].

2.2. Detonation waves

The situation encountered in such a case is well described in [11, 12, 4], thus we just present a schematic view of the problem in Fig. 1. In the inert case, see Fig. 1(a), the solution of the Riemann problem is either a shock wave or a rarefaction fan. When dealing with detonation waves, reactants may undergo a transition, provided the pressure is high enough, to give products at high pressure and temperature. Supposing that the reaction is infinitely fast, it is represented as a permeable front. Following the Chapman-Jouguet theory, this front appears as a wave which is always supersonic compared to the reactants and either supersonic or sonic compared to the products. It means that in the half Riemann problem, the four configurations represented in Fig. 1 are possible.

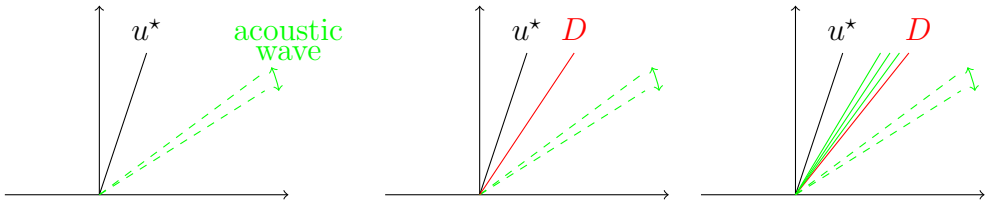


(a) Inert case. (b) Detonation case.

Figure 1: Half-Riemann problem with detonation waves. In the inert case, the waves pattern involve either a shock wave (left) or rarefaction waves (right). In the reactive case, we have an additional wave (red) which is either a superdetonation (left) or a CJ detonation front followed by an expansion wave (right).

2.3. Phase transition waves

Here again, we will briefly describe the phenomenon and refer to [13, 14] and references therein for a further description. As before, the phase transition is modeled by a permeable front. Yet, in this case, this one is always subsonic with respect to both of the phases. Moreover, contrary to the perfect gas eos case, the van-der-Waals eos is not strictly convex. Therefore, it induces two sonic waves which can be composite, as for example with under-compressive discontinuity attached with a rarefaction wave. See [14] or [13, pp.13–44] for a complete description of these composite waves. The situation is here summarized in Fig. 2.



(a) Single attached wave. (b) Single phase transition wave. (c) Phase transition wave followed by an expansion.

Figure 2: Half-Riemann problem with phase transitions. We may have the case 2(a) where the right wave (green) is either a shock wave or a rarefaction wave or an attached wave, the case 2(b) where the pure fluid wave can be followed by a phase transition wave (red) at the velocity D if the right state was initially a liquid phase, the case 2(c) where the phase transition wave (red) is followed by a rarefaction wave in the vapor.

3. Numerical scheme

In [2], it was proposed to avoid the modeling of the interfacial terms in the average model (1) and to start the discretization for the discrete equations instead. This idea has been developed for the inert case in a discontinuous Galerkin framework in [1], and is briefly recalled hereafter.

3.1. Inert Case

General formulation. Our numerical scheme is based on the ideas of [3] for the dG formulation of the non-conservative products and of [2] for the multiphase flow modeling. Following [15], for a given flow topology, each fluid obeys the following equation:

$$\chi_k \left(\partial_t \mathbf{U}_k + \mathrm{div}\mathbf{F}_k(\mathbf{U}_k)\right) = 0 \qquad \partial_t \chi_k + \mathbf{u}_i \cdot \nabla \chi_k = 0 \tag{2}$$

where $\mathbf{F}_k$ is the Eulerian flux computed with the eos of phase k, $\mathbf{u}_i$ is the local interface velocity, and χ_k is the characteristic function (it is equal to 1 if phase k is present and to 0 otherwise), which is known for the given flow topology. Combining these two sets of equations, we may obtain:

$$\frac{\partial\, \chi_k \mathbf{U}_k}{\partial\, t} + \mathrm{div}\left(\chi_k \mathbf{F}_k(\mathbf{U}_k)\right) - \left(\mathbf{F}_k(\mathbf{U}_k) - \mathbf{u}_i \mathbf{U}_k\right) \nabla \chi_k = 0 \tag{3}$$

Here, we may note that an average of Eq. (3) may lead to the Baer and Nunziato model (1) [15].

Let us consider now an open set Ω meshed by a conforming mesh $\mathcal{T}_h$. We define one unitary normal $\mathbf{n}$ on each side $S \in S_t$ of $\mathcal{T}_h$, where the set of sides $S_t = S_i \cup S_b$ involves interior sides S_i and boundary sides S_b. Applying the framework of [3], we find in [1] the following dG formulation (*without* numerical fluxes), which has been averaged among the different flow topologies:

$$\frac{\partial\, \mathbb{E}\left\{\chi_k \mathbf{U}_k\right\}}{\partial\, t} + \sum_{K \in \mathcal{T}_h} \int_K - \mathbb{E}\left\{\chi_k \mathbf{F}(\mathbf{U})\right\} \nabla \varphi + \varphi \left(\mathbb{E}\left\{(\mathbf{F} - \mathbf{u}_i \mathbf{U}) \nabla \chi_k\right\}\right) \tag{4}$$

$$- \sum_{S \in S_i} \int_S [\![\, \varphi \,]\!] \left\{\!\!\left\{ \mathbb{E}\left\{\chi_k \mathbf{F}_k(\mathbf{U}_k)\right\} \right\}\!\!\right\} \cdot \mathbf{n}^S \tag{5}$$

$$+ \sum_{S \in S_i} \int_S \left\{\!\!\left\{ \varphi \right\}\!\!\right\} \int_0^1 \frac{\partial \Phi}{\partial s}(s, u^L, u^R) \mathbb{E}\left\{(\mathbf{F}_k(\mathbf{U}_k) - \mathbf{u}_i \mathbf{U}_k)\right\} \cdot \mathbf{n}^S \tag{6}$$

$$+ \sum_{S \in S_b} \int_S \varphi \mathbb{E}\left\{\chi_k \mathbf{F}(\mathbf{U})\right\} \cdot \mathbf{n}^{\mathrm{out}} = 0 \tag{7}$$

where $\mathbb{E}$ is a mathematical expectancy, Φ a path connecting the left state L and the right state R and with $[\![\,\varphi\,]\!] = \varphi^R - \varphi^L$ and $\{\!\{\,\varphi\,\}\!\} = \dfrac{\varphi^R + \varphi^L}{2}$.

Boundary integrals. In this paragraph, we apply [2] for the boundary fluxes because it avoids to explicitly derive the jump relations for the non-conservative products. We found in [1] for the terms (5) and (6):

$$\int_S [\![\,\varphi\,]\!]\,\{\!\{\,\mathbf{F}(\mathbf{U})\,\}\!\}\cdot\mathbf{n}^S \approx \int_S [\![\,\varphi\,]\!]\mathcal{F}^{k,\mathrm{eul},+} \tag{8}$$

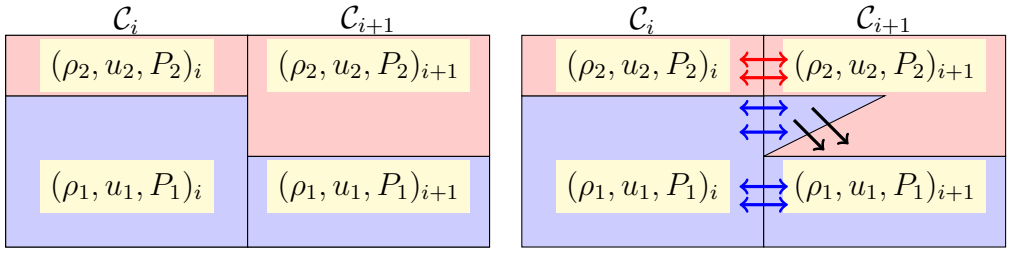
$$\int_S \{\!\{\,\varphi\,\}\!\}\int_0^1 \frac{\partial\Phi}{\partial s}(s,u^L,u^R)\,(\mathbf{F}_k(\mathbf{U}_k)-\mathbf{u}_i\mathbf{U}_k)\cdot\mathbf{n}^S \approx \int_S \varphi^L\mathcal{F}^{k,\mathrm{lag},-} + \int_S \varphi^R\mathcal{F}^{k,\mathrm{lag},+} \tag{9}$$

where $\mathcal{F}^{k,\mathrm{eul},+}$ and $\mathcal{F}^{k,\mathrm{lag},\pm}$ are average of Eulerian and Lagrangian fluxes that we detail now. The discretization of [2] is based on averaging the fluxes integrated from Riemann problems between pure fluids on a side. As depicted in Fig. 3, the first step to define the flux on a side is to solve the three possible Riemann problems. Then, these Riemann problems are integrated considering the various interfaces. For example in Fig. 3, the integration of the homogeneous Riemann problems lead to classical Eulerian fluxes whereas the integration of the heterogeneous Riemann problem strongly depends on the interfacial velocity: it leads to an Eulerian flux on the fluid that lies on the side and to a Lagrangian flux on both phases which is added on the cell in which the interface is. Last, all these fluxes are averaged by the occurrence's probability of each Riemann problem (see [2, pp 373-376]).

Cell integrals. Now, we are interested in the expression of the term (4). Usually, a continuous formulation of the system is known. Therefore, this step is straightforward. Here, on the contrary, we first defined the boundary integrals in the previous paragraph. Consequently, we have to find a continuous formulation of the problem which is consistent with our definition of the boundary integrals. Based on [1], we found:

$$\mathbb{E}\left\{(\mathbf{F}(\mathbf{U})-\sigma\mathbf{U})\cdot\nabla\chi_1\right\} = \begin{pmatrix} 0 \\ -P^\star(\nabla\alpha_1)\mathbf{n}(\nabla\alpha_1)\,\|\nabla\alpha_1\| \\ -u^\star(\nabla\alpha_1)P^\star(\nabla\alpha_1)\,\|\nabla\alpha_1\| \end{pmatrix} \tag{10}$$

where $\mathbf{n}(\nabla\alpha_1)$ is the unitary vector that has the same sense and direction as $\nabla\alpha_1$, $P^\star$ and $u^\star$ are the pressure and velocity at the interface of the Riemann



(a) Initial configuration. (b) Configuration after time evolution.

Figure 3: Configuration of the Riemann problem on a side between two adjacent cells. Each cell is filled, area corresponding to the volume fraction, by fluid 1 (blue) or 2 (red). Given the initial configuration 3(a),three Riemann problems shall be considered: 1-1, 1-2 and 2-2. The Riemann problem 2-1 was not represented because its weight is zero. On 3(b), after solving the different Riemann problems, only the contact discontinuity between different materials is represented. Integration of homogeneous Riemann problems leads to classical Eulerian fluxes (blue and red arrows). In our case, concerning the heterogeneous Riemann problem, the blue fluid is entering the right cell. Thus its integration leads to an Eulerian flux on the side for the blue fluid and to a Lagrangian flux (black arrows) on both the blue and red fluids in the right cell (expressing the fact that the blue fluid is pushing the red fluid in the right cell).

problem with direction $\mathbf{n}$ (left state corresponding to fluid 2 and right state to fluid 1).

3.2. Reactive case

As mentioned earlier, we suppose that the reactive fronts may be regarded as discontinuous waves and, therefore, the source terms are treated through a reactive Riemann problem (see Fig. 1 and 2). The integration of the three previous Riemann problems is now modified since we consider that the fluid 2 may react to give fluid 1. The system (4) – (7) still holds, Eulerian fluxes being unchanged, but the expression of boundaries integrals (9) and interior nonconservative cell integral (10) are modified. Indeed, χ_k has jump not only on interfaces, but also through transition waves: as shown in Fig. 4, the interactions 2-2 and 1-2 may lead to the apparition of a permeable front which induces the apparition of phase 1 (represented in green so as to differ it from the initially present fluid in blue) and therefore a jump of χ_k.

Boundary Integrals. A flux associated with a mass transfer will be called a "reactive" flux. As depicted in [1, p. 4105], the contribution of each type of

flux on each side is the average of the flux associated to pure phase Riemann problems:

$$\tilde{F}^{k,type,+} = \sum_{i,j} \mathbb{P}(i,j)\, \mathcal{F}_{ij}^{k,type,+} \qquad \text{and} \qquad \tilde{F}^{k,type,-} = \sum_{i,j} \mathbb{P}(i,j)\, \mathcal{F}_{ij}^{k,type,-}$$

where "*type*" is either Lagrangian, Eulerian or reactive. A reactive front may appear only in the case of a $2-2$, $1-2$ or $2-1$ Riemann problem. If such a front exists between phase i and j, integration of the equation (2) leads to:

$$\left\{ \begin{array}{l} \mathcal{F}_{ij}^{i,reac} = \mathbf{F}_i(\mathbf{U}_i^{reac}) - D\mathbf{U}_i^{reac} \\ \mathcal{F}_{ij}^{j,reac} = -\left(\mathbf{F}_i(\mathbf{U}_i^{reac}) - D\mathbf{U}_i^{reac}\right) \end{array} \right. \tag{11}$$

where D is the front velocity and superscript $reac$ stands for the state just in front of the reaction. Note that in the right hand side of (11), subscripts i and j can be replaced since Rankine–Hugoniot relations hold through the front. Last, the flux is added on the left (resp. right) cell depending on the sign of D:

$$\left\{ \begin{array}{l} \mathcal{F}_{ij}^{k,reac,+} = \mathrm{sgn}(D)\mathcal{F}_{ij}^{k,reac} \\ \mathcal{F}_{ij}^{k,reac,-} = \mathrm{sgn}(-D)\mathcal{F}_{ij}^{k,reac} \end{array} \right.$$

Cell integrals. As for the boundary integrals, the jump of χ_k must now be taken into account. This jumps affects the second part of (4), for which (10) does not hold any more. Reasoning as in [1], this value depends only on values of the Riemann problem between fluid 2 and 1 solved in the direction of $\nabla\alpha_1$. If this Riemann problem is not reactive, then (4) holds. Otherwise the problem is reactive, and χ_k jumps through the reactive wave. Then, taking the same notations as in the previous paragraph, we have:

$$\mathbb{E}\left\{(\mathbf{F}(\mathbf{U}) - \sigma\mathbf{U}) \cdot \nabla\chi_1\right\} = \left(\mathbf{F}_1(\mathbf{U}_1^{reac}(\nabla\alpha_1)) - D^{reac}(\nabla\alpha_1)\mathbf{U}_1^{reac}(\nabla\alpha_1)\right) \|\nabla\alpha_1\|$$

Here again, the subscript 1 of $\mathbf{F}$ and $\mathbf{U}$ can be changed to 2, because Rankine-Hugoniot relations hold through the reactive wave.

4. Results and discussions

A strong stability preserving (SSP) scheme [16] is used for the time discretization. In the present examples, spectral basis of Legendre (in one dimension) and of Dubiner (with triangles in two dimensions) are used. Finally, we use the classical minmod limiter so as to limit either the volume fraction if we have an interface ($0 < \alpha < 1$) or the characteristic variables if we have a pure fluid.

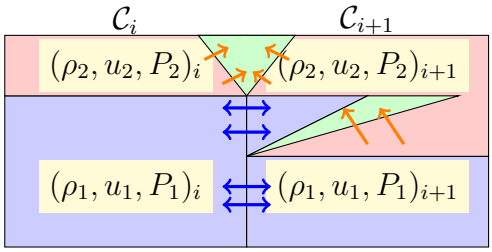
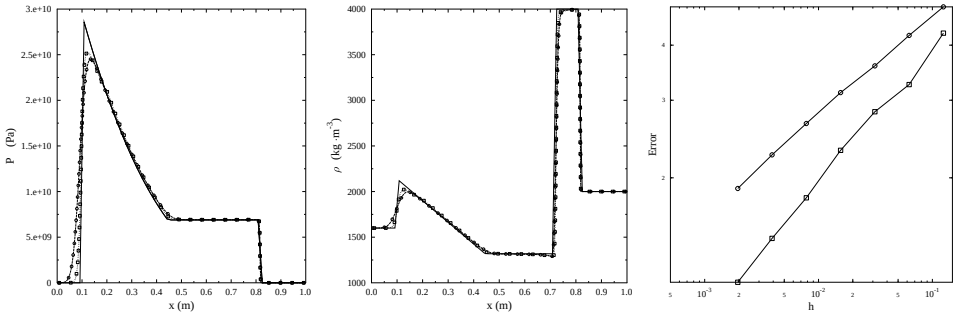


Figure 4: Configuration of the reactive Riemann problem on a side between two adjacent cells. A reactive front is responsible for the disappearance of fluid 2 which reacts to form a new state composed of fluid 1 (green).

4.1. Detonation waves

Our first example is a one-dimensional detonation inspired by [4]. A solid explosive at rest, denoted by r, is impacted at $x = 0.7\,\mathrm{m}$ by its gaseous products, denoted by p, at a velocity of $-1000\,\mathrm{m}\cdot\mathrm{s}^{-1}$. Initially, the pressure is uniform and at $10^5\,\mathrm{Pa}$ whereas the densities are $\rho_r = 1600\,\mathrm{kg}\cdot\mathrm{m}^{-3}$ and $\rho_p = 2000\,\mathrm{kg}\cdot\mathrm{m}^{-3}$. The two materials are governed by the reactive stiffened gas equation of state $P = (\gamma_i - 1)\,\rho\,(e - q_i) - \gamma P_{\infty,i}$, with $\gamma_r = 4$ and $P_{\infty,r} = 3{\cdot}10^9\,\mathrm{Pa}$ and $q_r = 4.56{\cdot}10^6\,\mathrm{J}{\cdot}\mathrm{kg}^{-1}$, $\gamma_p = 3$ and $P_{\infty,p} = 0\,\mathrm{Pa}$ and $q_p = 0\,\mathrm{J}{\cdot}\mathrm{kg}^{-1}$. The mesh contains 500 cells and the results are presented at $t = 70\,\mu\mathrm{s}$, for finite elements discretization of order 0 and 1. The numerical solution is thus compared to the exact one in Fig. 5, and a convergence study is also presented in Fig. 5(c). In this test case, we have two major difficulties. First, the detonation front is comparable to a shock immediately followed by an expansion wave where a fluid has appeared. It implies that the limitation process switches from the characteristic variables to the volume fraction in a very thin zone. Moreover, the solution is quite hard to compute since we have a spike of pressure immediately followed by a decrease in pressure. In such case, if we use a non-monotone limiter, the scheme fails to determine the correct state (velocity of the detonation front, CJ state...), as shown in Fig. 6, and that is why our computations were made with a monotone limiter. This behavior is of particular importance to be mentioned. The need for a monotone limiter can be understood as follows. In the original numerical scheme [2], the weights depend on the sign of $\nabla\alpha_k\cdot\mathbf{n}$ where $\mathbf{n}$ is the normal to the side. In the consistent continuous limit found in [1], expressions of $\mathbf{u}_I$ and P_I, which are $\mathbf{u}_I = u^\star(\nabla\alpha_1)\mathbf{n}(\nabla\alpha_1)$ and $P_I = P^\star(\nabla\alpha_1)$, depend singularly

on the sign of $\nabla\alpha_1$. For example, in one dimension, P_I and u_I switch from the interfacial pressure and velocity of the Riemann problems $1-2$ and $2-1$ when the sign of $\partial_x\alpha_1$ changes. Consequently, it is important that $\partial_x\alpha_1$ remains monotone at the discrete level. We point out that as the singularity depends only on $\nabla\alpha_1$, the requirement of a monotone limiter lies only on the volume fractions. In the reactive case, the problem has essentially the same origin, except that it is also involved with the reactive front, for which the continuous limit is harder to express. Eventually, we may see that even if the solution is not excellent, the high order slightly increases the solution: the detonation front is less diffuse, the spike and the inert shocked state are better described. Furthermore, we have a better order of accuracy.

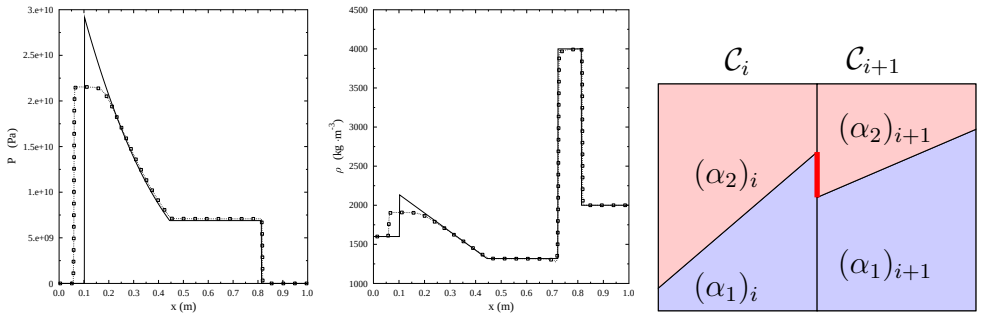


(a) Pressure profiles. (b) Density profiles. (c) Convergence order.

Figure 5: 1D detonation. dG^0 (circle), dG^1 (square) and exact (line) solutions.

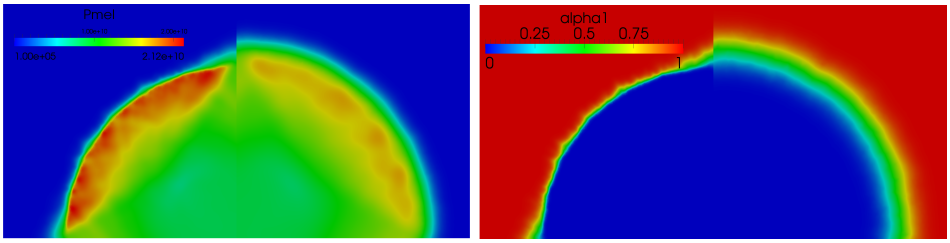
Our second example is a two-dimensional detonation front. It concerns the ignition of an explosive, contained in a rectangular tank, in its center. The ignition mechanism is out of scope of our study, so we replace it by a "bubble" of products at high pressure ($P = 10^{10}$ Pa). The EOS parameters are identical to the previous ones. The problem being symmetric, we meshed only a quarter of the rectangle with an unstructured triangular mesh containing 855 cells. In Fig. 7, we compare the dG^0 and the dG^1 solutions at $t = 55\,\mu$s. It may clearly be seen that the spike of the detonation is better described with the dG^1 scheme. Moreover, the reaction zone is also much better resolved.

4.2. Phase transition waves



(a) Pressure profiles. (b) Density profiles. (c) Configuration of the Riemann problem on a frontier.

Figure 6: 1D detonation. Incorrect solutions obtained with a non-monotone limiter. As shown on Fig. 6(a) and 6(b), the numerical scheme might converge to a wrong solution if a non-monotone limiter is used. Origin of the problem is shown on Fig. 6(c): the non-monotone behavior of the limiter induces a blue-red Riemann problem (represented by a strong line in red), which does not match with the physical reaction which is normally driven by reactive red-blue Riemann problems.



(a) Pressure profiles. (b) Volume fraction of reactants.

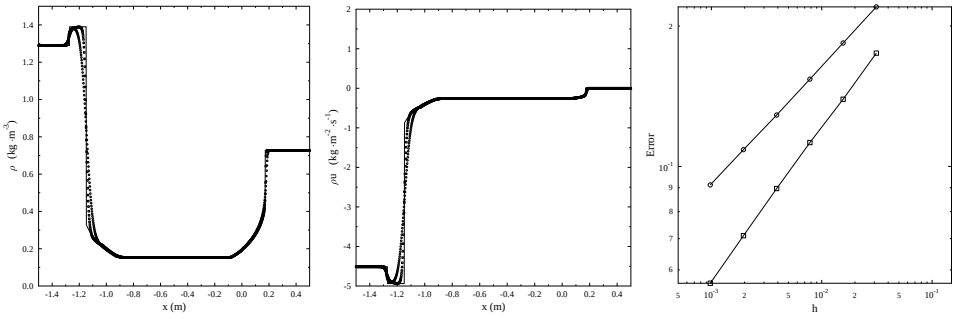
Figure 7: 2D detonation. Comparison of the dG^1 (left) and the dG^0 (right) solutions.

An adimensional form of the van-der-Waals equation of state is now used:

$$P(\rho) = \frac{8\,T\rho}{3-\rho} - 3\,\rho^2 \qquad 0 < \rho < 3 \tag{12}$$

As in [17], what seems to be a one phase problem is transformed into a multiphase problem: during the computations, low (resp. high) densities, i.e. below (resp. above) the spinodal zone, stand for the liquid (resp. gas) phase. Nonuniqueness issue of the solution of the Riemann problem is solved as in [14]. In this framework, following [17], a wave that links two states on both sides of the spinodal zone is considered as a reactive front.

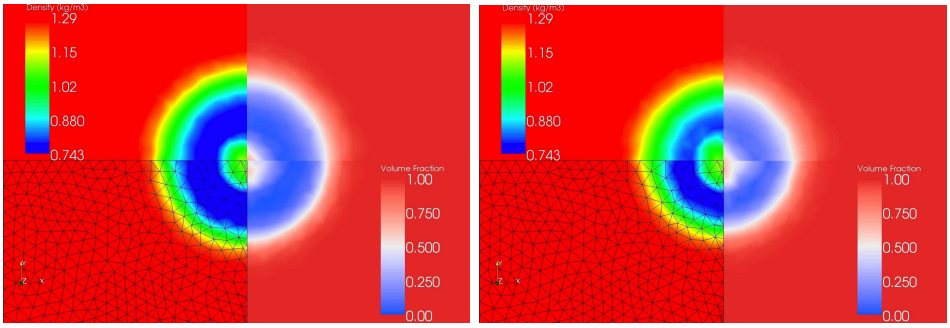
Our first example is a Riemann problem, proposed by [14], [13, p.119]. Temperature is set to 0.9. An interface separates two fluids whose densities are taken at their Maxwell values. The left part is at rest, the right part has initially a velocity $u = -3.5\,\mathrm{m}\cdot\mathrm{s}^{-1}$. The mesh contains 1000 cells. Results at $t = 0.3\,\mu$s are shown in Fig. 8. Here again, a convergence test is proposed in Fig. 8(c). This test is hard to handle since we have a shock followed by a phase transition at left and an attached wave, i.e. a discontinuity followed by a rarefaction wave, at right. We may see that this dG extension of the method [17] has no problem to deal with such a complicated waves configuration and with the apparition of a phase. Furthermore, we may note that we have a qualitatively good agreement with the exact solution for both methods. Besides, the dG^1 scheme really improves the solution, see Figure 8(c).



(a) Density profiles. (b) Momentum profiles. (c) Convergence order.

Figure 8: 1D phase transition. dG^0 (circle), dG^1 (square) and exact (line) solutions.

Our second example is a two-dimensional test taken from [17]. It deals with the collapse of a metastable bubble of vapor in its associated liquid. We use an unstructured mesh composed of 855 triangles. In Fig. 9, we show a sequence of the density and volume fraction of liquid for the dG^0 and the dG^1 solution. Once more, we may see that even with a coarse mesh, the method gives acceptable results and we have a clear boon with the DG^1 scheme.



(a) $t = 3\,\mathrm{s}$. (b) $t = 5\,\mathrm{s}$.

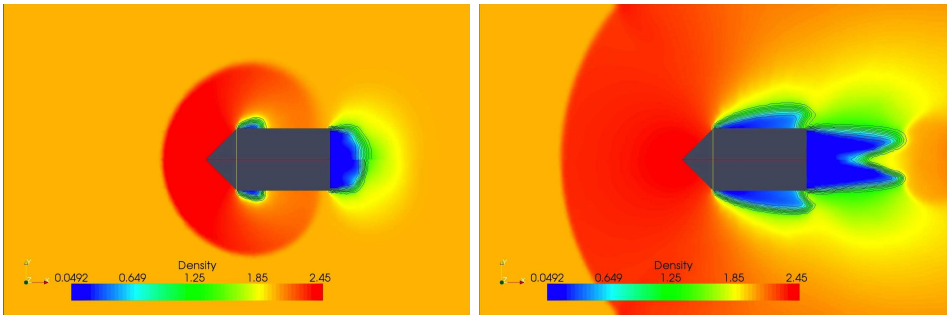
Figure 9: 2D phase transition: collapse of a metastable bubble. Density (left) and volume fraction (right) profiles for the dG^0 (top) and the dG^1 (bottom) solutions.

Finally, our last example concerns the propagation of a projectile in a liquid tank. A rectangular domain, initially at atmospheric pressure, filled by a liquid with a density $\rho = 2\,\mathrm{kg}\cdot\mathrm{m}^{-3}$ contains a projectile moving at $-2\,\mathrm{m}\cdot\mathrm{s}^{-1}$. The mesh is composed of 8024 triangles. We show the time evolution of the density in Fig. 10.

The method is able to deal with the dynamic apparition of the gaseous phase. The dG^1 solution is still better, with a sharper interface.

5. Conclusion

We have presented how to develop a discontinuous Galerkin method for a reactive compressible multiphase flow. The source terms were treated through a reactive Riemann problem, enhanced by new waves corresponding to the reactive fronts. The scheme is average conservative. Several reactive tests have been presented, either one-dimensional or two-dimensional. They all show the high capabilities of the method, especially it has no difficulty



(a) $t = 0.06\,\mathrm{s}$. (b) $t = 0.17\,\mathrm{s}$.

Figure 10: 2D phase transition: projectile moving in a liquid. Density profiles for the dG^0 (top) and the dG^1 (bottom) solutions, with gas volume fractions isovalues (black lines).

whenever a particular phase appears or disappears. The results show yet that the limitation of the high order scheme is not straightforward, because a monotone limiter is required. A thorough study of this issue shall be considered.

[1] E. Franquet, V. Perrier, Runge-Kutta discontinuous Galerkin method for the approximation of Baer & Nunziato type multiphase model, Journal of Computational Physics 231 (2012) 4096–4141.

[2] R. Abgrall, R. Saurel, Discrete equations for physical and numerical compressible multiphase mixtures, Journal of Computational Physics 186 (2003) 361–396.

[3] S. Rhebergen, O. Bokhove, J. J. W. van der Vegt, Discontinuous Galerkin finite element methods for hyperbolic nonconservative partial differential equations, J. Comput. Phys. 227 (3) (2008) 1887–1922. doi:10.1016/j.jcp.2007.10.007.

[4] O. Le Métayer, J. Massoni, R. Saurel, Modelling evaporation fronts with reactive Riemann solvers, Journal of Computational Physics 205 (2005) 567–610.

[5] M. Baer, J. Nunziato, A two-phase mixture theory for the deflagration-to-detonation transition (DDT) in reactive granular materials, Int. J. Multiphase Flows 12 (12) (1986) 861–889.

[6] I. Toumi, A. Kumbaro, An approximate linearized Riemann solver for a two-fluid model, Journal of Computational Physics 124 (2) (1996) 286 – 300.

[7] R. Saurel, R. Abgrall, A simple method for compressible multifluid flows, SIAM J. Sci. Comput. 21 (3) (1999) 1115–1145.

[8] F. Coquel, T. Gallouët, J. Hérard, N. Seguin, Closure laws for a two-fluid two-pressure model, C. R. Acad. Sci. Paris I 334 (2002) 927–932.

[9] B. Cockburn, C.-W. Shu, Runge-Kutta discontinuous Galerkin methods for convection-dominated problems, J. Sci. Comput. 16 (3) (2001) 173–261. doi:10.1023/A:1012873910884.

[10] C. Wang, X. Zhang, C.-W. Shu, J. Ning, Robust high order discontinuous Galerkin schemes for two-dimensional gaseous detonations, Journal of Computational Physics 231 (2) (2012) 653 – 665.

[11] W. Fickett, W. Davis, Detonation, University of California Press, Berkeley, CA, 1979.

[12] A. Godlewski, P.-A. Raviart, Numerical approximation of hyperbolic systems of conservation laws, springer-verlag Edition, Vol. 118 of Applied Mathematical Sciences, 1996.

[13] C. Merkle, Dynamical phase transitions in compressible media, Ph.D. thesis, Albert-Ludwigs-Universität Freiburg, available at http://www.freidok.uni-freiburg.de/volltexte/2674/ (2006).

[14] C. Merkle, C. Rhode, The sharp-interface approach for fluids with phase change: Riemann problems and ghost fluid techniques., M2AN Math. Model. Numer. Anal. 41 (6) (2007) 1089–1123.

[15] D. Drew, S. Passman, Theory of multicomponent fluids, Vol. 135 of Applied Mathematical Sciences, Springer-Verlag, New York, 1999.

[16] S. Gottlieb, C.-W. Shu, E. Tadmor, Strong stability-preserving high-order time discretization methods, SIAM Rev. 43 (1) (2001) 89–112.

[17] V. Perrier, A conservative method for the simulation of the isothermal Euler system with the van-der-Waals equation of state, Journal of Scientific Computing 48 (296-303).